Dynamic Modeling of Biogas Upgrading in Hollow Fiber Membrane Contactors

ARTICLE *in* ENERGY & FUELS · SEPTEMBER 2014

Impact Factor: 2.79 · DOI: 10.1021/ef501435q

5 AUTHORS, INCLUDING:

Yunfei Yan
Chongqing University
34 PUBLICATIONS **122** CITATIONS
SEE PROFILE

Zhien Zhang
Chongqing University
21 PUBLICATIONS **60** CITATIONS
SEE PROFILE

energy&fuels

Article

pubs.acs.org/EF

Dynamic Modeling of Biogas Upgrading in Hollow Fiber Membrane Contactors

Yunfei Yan,*,† Zhien Zhang,† Li Zhang, Yanrong Chen, and Qiang Tang

Key Laboratory of Low-Grade Energy Utilization Technologies and Systems, Ministry of Education, Chongqing University, Chongqing 400044, People's Republic of China

ABSTRACT: Membrane absorption is a novel method for acid gas removal compared to conventional separation techniques. The current study presents the simulation results using a computational fluid dynamics (CFD) method for biogas purification. A comprehensive two-dimensional (2D) mass-transfer model was developed and solved in a hollow fiber membrane contactor (HFMC) under a non-wetted condition. H_2O, triethanolamine (TEA), diethanolamine (DEA), monoethamolamine (MEA), and potassium arginate (PA) were used as the absorbent liquids. The effects of gas−liquid parameters and membrane characteristics on the CO_2 removal efficiency and absorption flux and CH_4 recovery were systematically examined and evaluated. The comparisons between model predictions and experimental data with various gas−liquid parameters were in good agreement. An increase of gas velocity and CO_2 content caused an increase of CO_2 flux and a decrease of CO_2 removal efficiency and CH_4 recovery; however, an increase of absorbent velocity and concentration caused an increase in the above three values. In addition, a smaller fiber inner diameter and membrane thickness and a longer module were good for the biogas upgrading process. It should be noted that the highest CO_2 flux coincided with the original module dimensions. The simulation predictions also showed that PA provided better membrane module performance than other absorbents. The order for CO_2 absorption efficiency and CH_4 recovery was PA > MEA > DEA > TEA > H_2O. Overall, the developed model provides the guidelines for selecting the optimum module properties and fluid conditions. The membrane gas absorption technique has shown great potential in biogas upgrading.

1. INTRODUCTION

With the rapid development of technology, there is an increasing demand for fuels. Natural gas is an environmentally friendly, renewable, and clean energy source. It is also the third largest proportion in energy structure throughout the world after coal and oil. Biogas production and utilization is an additional available energy. The upgraded biogas in the form of a natural gas candidate can be supplied to the developed natural gas grids and delivered to industry and households. Particularly, it can be used as a vehicle fuel, of which the demand has dramatically increased over the past few decades.[1,2] The separation of CH_4 and CO_2 is a key issue in the natural gas industry. Generally, there are several techniques for CO_2 capture from biogas, i.e., physical and chemical absorption, pressure swing adsorption, membrane separation, etc.[3] Among them, the membrane gas absorption (MGA) has been introduced to be a high-efficiency technique and promising alternative for conventional separation methods for acid gas removal.[4−6] This process combines the advantages of both chemical absorption and membrane separation methods, including no channeling, flooding, entraining, and foaming issues, less capital investment, much bigger gas−liquid interfacial area, and ease to scale up.[4]

The main CO_2 emission is produced from fossil fuel combustion and other industrial processes. There are various sources of CO_2 emissions worldwide, which result in global warming. With regard to pure CO_2, Boributh et al.[7] investigated the physical absorption of CO_2 considering pore size distribution and wetting ratio in a hollow fiber membrane module. Zhang et al.[8] reported that the CO_2 removal efficiency for single gas reached around 95% when monoethamolamine (MEA) solution was used as the absorbent. These investigations indicated that the membrane gas absorption method for pure CO_2 capture was feasible when using the appropriate absorbent. In terms of flue gas, CO_2 accounts for about 10−20% in the gas mixture. Mehdipour et al.[9] studied flue gas containing 20% CO_2 and 80% N_2 as the research object. The CO_2 capture process reached complete removal using 2 M K_2CO_3 solution at 298 K. Furthermore, Masoumi et al.[6] analyzed CO_2 absorption from gas mixtures containing 10% CO_2 into MEA/diethanolamine (DEA)/*N*-methyldiethanolamine (MDEA)-promoted potassium carbonate solutions in a membrane contactor. They showed that the CO_2 flux increased considerably using promoted solutions in comparison to non-promoted solutions. In the case of natural gas, CO_2 also accounts for a major proportion. Keshavarz et al.[10] simulated a feed gas mixture of 15% CO_2, 5% H_2S, and 80% N_2 absorption in a membrane module. They successfully conducted the simultaneous absorption of CO_2 and H_2S in a mass-transfer model. For the first time, Marzouk et al.[11,12] carried out experiments on CO_2 removal from a gas mixture containing 90.5% CH_4 and 9.5% CO_2 into water and amine solvents at high pressures up to 50 MPa in a hollow fiber membrane contactor (HFMC). Thus, plenty of researchers have paid close attention to the applications of membrane contactors for CO_2 capture from pure CO_2, flue gas, or natural gas. Typically, there is 25−50% CO_2 in the composition of biogas. However, CO_2 absorption from biogas in a HFMC is rarely reported in the published literature.[3]

Lately, a variety of aqueous solvents, including physical and chemical solutions, have been widely investigated experimentally and theoretically. Choosing an appropriate absorbent liquid is a significant factor influencing the membrane performance. Physical solvent has low capital compared to the expensive

Received: June 27, 2014
Revised: August 11, 2014
Published: August 12, 2014

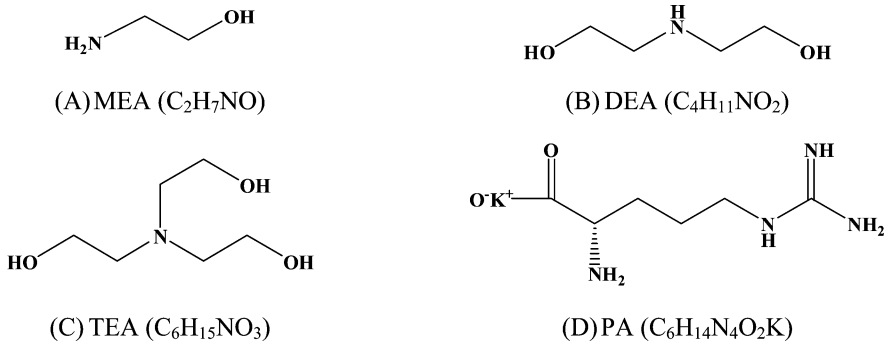

Figure 1. Molecular structures for different liquid absorbents used in this simulation.

chemical solvent for CO_2 absorption. Porcheron and Drozdz[13] carried out experiments and modeling of the gas–liquid contact process using H_2O as the solvent in a polypropylene (PP) HFMC. However, the CO_2 absorption effect under these conditions was not obvious. Rangwala[14] compared the CO_2 absorption performance of three absorbents: aqueous H_2O, NaOH, and DEA solvents using HFMCs. The mass-transfer rate for absorption of CO_2 in the HFMC was examined. The results showed that the removal process was significantly enhanced in the case of chemical absorption compared to physical absorption. This was due to the reason that the amine solutions were weak basic compounds and the chemical bonds between amine and CO_2 were easily broken under high temperatures. To improve the reaction rate constant, the mixed solutions using activators into the absorbent have gained wide attention. Lin et al.[15] investigated blended solutions of piperazine (PZ) and 2-amino-2-methyl-1-propanol (AMP) in the gas absorption membrane process. They found that increasing the PZ concentration showed an increase of the CO_2 absorption rate. Furthermore, Munoz et al.[16] tested new liquid absorbents consisting of water solutions of CO_2-complexing agents, and the absorbents showed outstanding absorption capacities, superior to MEA or any other amino acid. However, it is necessary to find a novel aqueous absorbent with higher surface tension and lower reaction heat, because the alkanolamine solutions result in membrane wetting issues. It was noted that amino acid salts were good substitutes for conventional solutions because they had higher surface tension, which reduced the risk of membrane wetting. The solvents based on amino acid salts were also suitable for stable and long-term gas–liquid reaction in the membrane module.[17,18]

Recently, a number of simulation works have been accomplished to explore the behaviors of gas transport in the membranes. Keshavarz et al.[10,19] developed a steady-state model and numerical scheme for CO_2 separation in a HFMC under non-wetted and partially wetted modes. The reversible chemical reactions in the liquid phase as well as wetted parts of the pores were considered in the diffusion–reaction models. They indicated that the membrane performance was deteriorated with a high wetting ratio of the membrane. Additionally, a general two-dimensional (2D) mathematical model for calculation of the CO_2 concentration in polymeric membrane modules was established, which took into account axial and radial diffusion in the tube, membrane, and shell compartments of the contactor. The simulated predictions were in excellent consistency with the available experimental values for various liquid velocities.[20] Al-Marzouqi et al.[21,22] used a mass-transfer model to simulate the transport process of gas and liquid in the membrane contactor under the non-wetted conditions. Additionally, they found increasing the absorbent concentration and velocity or decreasing the gas velocity increased the CO_2 removal efficiency. Later, Jung et al.[23] used two models, including the explicit model and the multilayer perceptron neural network model for the CO_2 capture process using HFMCs. They stated that the explicit model for the single-stage module could be extended to the multistage module, and these models could be applied in CO_2 absorption in a HFMC. However, in most previous literature, there is no simulation work that simultaneously reported the effects of the fluid properties and module structure on the biogas purification efficiency in the HFMC. Also, from the above observations, the computational fluid dynamics (CFD) technique is a feasible method to predict acid gas removal in the contactor.

In the present study, a 2D mass-transfer model for simulation of CO_2 separation from biogas at atmospheric pressure was developed. The effects of gas and liquid properties and membrane structure were investigated by a simulated biogas containing 40% CO_2 and 60% CH_4. In the simulations, biogas and liquid flow countercurrently in a non-wetting condition. Physical solvent (H_2O) and chemical absorbents [triethanolamine (TEA), DEA, MEA, and potassium argininate (PA)] were used for CO_2 absorption. Among them, PA shows better absorption performance compared to other conventional absorbents because of several amino groups in the molecular structure (see Figure 1). It also provides the advantages of low volatility, ionic property, and resistance to oxidative and thermal degradation. It is the first time the aqueous PA solution was used as an absorbent in a HFMC. The governing equations including the tube, membrane, and shell regions are solved in the material balance. The validation of the developed model was verified with the experimental data by Yan et al.,[3] where the non-wetting condition was assumed.

2. THEORY

In this study, a numerical analysis of CO_2 separation from biogas in a HFMC is conducted by means of deriving and solving the continuity equations, including three domains: the gas, porous membrane, and absorbent sections. The schematic diagram of the gas–liquid membrane contactor is depicted in Figure 2. As can be seen, the biogas is fed into the shell side, passing through the membrane pores, and then is absorbed by aqueous liquid. Only the gas phase diffuses in the membrane because of operation in a non-wetted condition. In this case, the absorbent is passed into the tube in a countercurrent flow.

Specifications of the module used in this numerical analysis are shown in Table 1. The membrane module was provided by Hangzhou Jeffel Membrane Technology, Ltd. in China. The following assumptions are made in this simulation work: (1) steady state and isothermal conditions, (2) ideal gas behavior, (3) applicability of Henry's law for the gas–liquid interface,

dx.doi.org/10.1021/ef501435q | Energy Fuels 2014, 28, 5745–5755

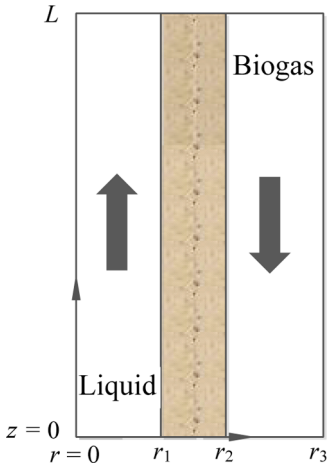

Figure 2. Schematic of a gas−liquid HFMC.

Table 1. Specifications of the Membrane Module[4]

parameter	value
membrane material	polypropylene (PP)
fiber inner diameter (μm)	360
membrane thickness (μm)	45
Happel's free surface model radius (μm)	402
module inner diameter (m)	3.6
membrane length (cm)	320
number of fibers	500
porosity	0.45
tortuosity	$(2-\varepsilon)/\varepsilon$
packing density	0.3125
membrane area (m^2)	0.176

(4) non-wetted mode for the membrane contactor, (5) laminar flow for gas and absorbent flow in the HFMC, and (6) a fully developed laminar parabolic velocity profile in the fibers.

2.1. Governing Equations Inside the Tube. Considering diffusion, reaction, and convection, the steady-state material balance equation for each species i (CO_2 or absorbent) in the tube side may be expressed below

$$D_{i\text{-tube}}\left[\frac{\partial C_{i\text{-tube}}}{\partial r}+\frac{1}{r}\frac{\partial C_{i\text{-tube}}}{\partial r}+\frac{\partial^2 C_{i\text{-tube}}}{\partial z^2}\right] = U_{z\text{-tube}}\frac{\partial C_{i\text{-tube}}}{\partial z}-R_i \quad (1)$$

where $D_{i\text{-tube}}$, $C_{i\text{-tube}}$, $U_{z\text{-tube}}$, and R_i are the diffusion coefficient and the concentration of species i inside the tube, the velocity in the axial direction, and the reaction rate, respectively. When physical absorption is considered in the membrane contactor, the reaction term in eq 1 is negligible. The axial velocity distribution in the tube is assumed to follow Newtonian laminar flow[24]

$$U_{z\text{-tube}} = 2\bar{U}_{\text{tube}}\left[1-\left(\frac{r}{r_1}\right)^2\right] \quad (2)$$

where $\bar{U}_{\text{tube}}$ denotes the average velocity in the tube side, r is the radial coordinate, and r_1 is the inner fiber radius.

2.2. Governing Equations Inside the Membrane. In the case of the non-wetted mode, the steady-state governing equation for CO_2 transport can be expressed as

$$D_{CO_2\text{-mem}}\left[\frac{\partial C_{CO_2\text{-mem}}}{\partial r}+\frac{1}{r}\frac{\partial C_{CO_2\text{-mem}}}{\partial r}+\frac{\partial^2 C_{CO_2\text{-mem}}}{\partial z^2}\right]=0 \quad (3)$$

where $D_{CO_2\text{-mem}}$ and $C_{CO_2\text{-mem}}$ are the diffusion coefficient and the concentration of CO_2 across the membrane, respectively.

The diffusion coefficient of CO_2 in the membrane considering the effect of porosity and tortuosity can be written as

$$D_{CO_2\text{-mem}} = \frac{\varepsilon}{\tau}D_{CO_2\text{-shell}} \quad (4)$$

where ε, τ, and $D_{CO_2\text{-shell}}$ denote the membrane porosity, the membrane tortuosity, and the diffusion coefficient of CO_2 inside the shell, respectively.

2.3. Governing Equations Inside the Shell. The differential mass-transfer balance for CO_2 transport in the shell is given by

$$D_{CO_2\text{-shell}}\left[\frac{\partial C_{CO_2\text{-shell}}}{\partial r}+\frac{1}{r}\frac{\partial C_{CO_2\text{-shell}}}{\partial r}+\frac{\partial^2 C_{CO_2\text{-shell}}}{\partial z^2}\right] = U_{z\text{-shell}}\frac{\partial C_{CO_2\text{-shell}}}{\partial z} \quad (5)$$

where $U_{z\text{-shell}}$ represents the axial velocity in the shell and $C_{CO_2\text{-shell}}$ is the CO_2 concentration inside the shell.

The gas flow in the shell side is always very complicated. Assuming Happel's free surface theory, the axial velocity inside the shell may be estimated as[25]

$$U_{z\text{-shell}} = 2\bar{U}_{\text{shell}}\left[1-\left(\frac{r_2}{r_3}\right)^2\right]\times\left[\frac{(r/r_3)^2-(r_2/r_3)^2+2\ln(r_2/r)}{3+(r_2/r_3)^4-4(r_2/r_3)^2+4\ln(r_2/r_3)}\right] \quad (6)$$

Table 2. Boundary Conditions of Governing Equations

boundary	tube	membrane	shell
$z=0$	$C_{CO_2\text{-tube}}=0$	insulated	$\frac{\partial C_{CO_2\text{-shell}}}{\partial r}=0$
$z=L$		insulated	$C_{1\text{-tube}}=C_0$
$r=0$	$\frac{\partial C_{CO_2\text{-tube}}}{\partial r}=0$		
$r=r_1$	$C_{CO_2\text{-tube}}=mC_{CO_2\text{-mem}}$ $\frac{\partial C_{1\text{-tube}}}{\partial r}=0$	$C_{CO_2\text{-mem}}=\frac{C_{CO_2\text{-tube}}}{m}$	
$r=r_2$		$C_{CO_2\text{-mem}}=C_{CO_2\text{-shell}}$	$C_{CO_2\text{-shell}}=C_{CO_2\text{-mem}}$

dx.doi.org/10.1021/ef501435q | Energy Fuels 2014, 28, 5745−5755

Table 3. Physicochemical Properties Used in This Study

parameter	value/expression	reference
R (m^3 atm mol^{-1} K^{-1})	8.314	26
D_{CO_2} (m^2 s^{-1})	1.8×10^{-5}	27
$D_{CO_2}^{mem}$ (m^2 s^{-1})	$1.8 \times 10^{-5}(\varepsilon/\tau)$	27
	CO_2-H_2O	
m_{H_2O}	0.83	28
$D_{CO_2}^{H_2O}$ (m^2 s^{-1})	$2.35 \times 10^{-6}\exp(-2199/T)$	29
$D_{H_2O}^{l}$ (m^2 s^{-1})	$0.5D_{CO_2}^{H_2O}$	30
	CO_2-MEA	
m_{MEA}	0.86	6
k_{MEA} (m^3 mol^{-1} s^{-1})	$10^{(10.99-2152/T)}/1000$	31
$D_{CO_2}^{MEA}$ (m^2 s^{-1})	1.4×10^{-9}	30
D_{MEA}^{l} (m^2 s^{-1})	7.7×10^{-10}	30
R_{MEA}	$k_{MEA}C_{CO_2}C_{MEA}$	30
	CO_2-TEA	
m_{TEA}	0.602	32
k_{TEA} (m^3 mol^{-1} s^{-1})	$4.52 \times 10^{4}\exp(-2688/T)$	33
$D_{CO_2}^{TEA}$ (m^2 s^{-1})	1.95×10^{-9}	34
D_{TEA}^{l} (m^2 s^{-1})	7.11×10^{-10}	34
R_{TEA}	$k_{TEA}C_{CO_2}C_{TEA}$	34
	CO_2-DEA	
m_{DEA}	0.8	30
k_2 (m^3 mol^{-1} s^{-1})	2.375	35
$k_2k_{H_2O}/k_{-1}$	2.2×10^{-6}	35
k_2k_{DEA}/k_{-1}	4.37×10^{-4}	35
H_2O concentration (mol m^{-3})	50	36
$D_{CO_2}^{DEA}$ (m^2 s^{-1})	1.05×10^{-9}	30
D_{DEA}^{l} (m^2 s^{-1})	4.97×10^{-10}	30
R_{DEA}	$\dfrac{C_{CO_2}C_{DEA}}{\frac{1}{k_2}+\frac{1}{(k_2k_{H_2O}/k_{-1})C_{H_2O}+(k_2k_{DEA}/k_{-1})C_{DEA}}}$	35
	CO_2-PA	
m_{PA}	0.66	37
k_{PA} (m^3 mol^{-1} s^{-1})	$(2.58 \times 10^{16}\exp(-8654/T)C_{Arg} + 4.32 \times 10^{13}\exp(-6666/T)C_{OH^-})C_{CO_2}$	38
OH^- concentration (mol m^{-3})	$K_w/K_p((1-m_{PA})/m_{PA})$	39 and 40
$D_{CO_2}^{PA}$ (m^2 s^{-1})	$D_{CO_2}^{H_2O}(\mu_{H_2O}/\mu_{PA})^{0.82}$	38
D_{PA}^{l} (m^2 s^{-1})	$0.5D_{CO_2}^{PA}$	30
$D_{CO_2}^{H_2O}$ (m^2 s^{-1})	$2.35 \times 10^{-6}\exp(-2199/T)$	38
μ_{H_2O} (mPa s^{-1})	$1.86 \times 10^{-6}\exp(16400/RT)$	38
μ_{PA} (mPa s^{-1})	1.276	37
R_{PA}	$k_{PA}C_{CO_2}C_{PA}$	38

where $\bar{U}_{shell}$, r_2, and r_3 are the average velocity in the shell, the outer fiber radius, and Happel's free surface model radius, respectively.

The boundary conditions for solving the developed mass-transfer model are listed in Table 2.

3. NUMERICAL SCHEME

The physical and chemical parameters used in this model are shown in Table 3. The finite difference element method is used for numerical solution of the governing equations (eqs 1, 3, and 5) using COMSOL Multiphysics software, version 4.4. The material balance error control and adaptive meshing are applied using a numerical solver of PARDISO, which is thread-safe, high-efficiency, robust, memory efficient, and easy to use for solving large sparse symmetric linear systems of equations on shared- and distributed-memory multiprocessors. A computational platform with the characteristics of RAM 4.00 GB and Intel Core i5-4200U CPU at 1.60 GHz and 64-bit operating system was used to solve the coupled partial differential equations. The computational time for solving the model equations was about 3 min.

4. RESULTS AND DISCUSSION

4.1. Concentration Distribution of Phases. Figure 3 shows the concentration gradients and flux vectors of CO_2 and liquid in the membrane contactor using 10 wt % PA solution as the absorbent while considering the non-wetting condition. The biogas is fed into the shell from the inlet of the shell ($z = L$), where the concentration of the gas mixture is maximum, while the absorbent flows from the inlet of the tube ($z = 0$), where the CO_2 concentration is assumed to be zero. It can be seen from Figure 3A that the concentration gradient and flux vectors of solvent in the center of the fiber are higher than those at the gas–liquid interface because of the absence of CO_2. The concentration gradient of liquid gradually decreases from the

dx.doi.org/10.1021/ef501435q | Energy Fuels 2014, 28, 5745−5755

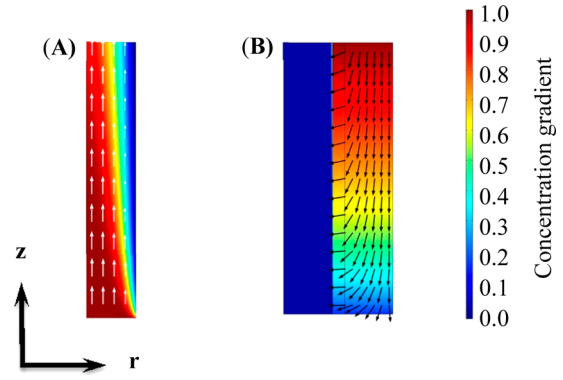

Figure 3. Two-dimensional concentration distribution of (A) absorbent and (B) CO_2 in the HFMC (liquid concentration, 10 wt %; T, 303 K; U_l, 0.06 m s^{-1}; and U_g, 0.32 m s^{-1}).

inlet to the outlet of the tube side. It is also indicated from Figure 3B that CO_2 flows across the membrane because of the large concentration difference between the feed and tube side and then is absorbed by the solvent inside the tube. The CO_2 flux vectors are in both r and z directions in the tube and shell sections because of diffusion and convection. In addition, the concentration gradient of CO_2 inside the tube is much smaller than that inside the shell and membrane domains because of the lower diffusion coefficient in the solvent than that in the gas phase. It is clearly seen that the CO_2 dimensionless concentration distribution is more uniform when the solvent passes through the tube side.

4.2. Concentration Profile in the Axial Direction. The axial CO_2 concentration profile at the membrane−shell interface of the membrane contactor with different solvents is depicted in Figure 4. It is obvious that the CO_2 concentration is maximum at

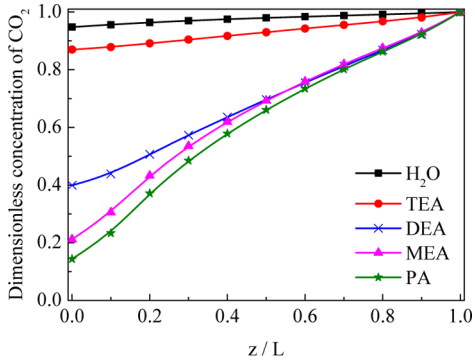

Figure 4. Concentration profile for CO_2 with various absorbents along the membrane module (liquid concentration, 10 wt %; T, 303 K; U_l, 0.06 m s^{-1}; and U_g, 0.32 m s^{-1}).

$z = L$ and then declined to the minimum at the outlet ($z = 0$) along the membrane module in the shell side. The amount of CO_2 in the gas mixture is increasingly absorbed by the aqueous solvent. It is also noted that PA solution is the best solvent for CO_2 separation, and the value of the dimensionless concentration at $z = 0$ is around 0.1. This contributed to the highest reaction rate with CO_2. In addition, water and TEA show bad absorption performance. The sequence of absorption performance for all of the solvents is H_2O < TEA < DEA < MEA < PA.

4.3. Effect of Gas−Liquid Properties (Model Validation). *4.3.1. Effect of the Gas Velocity.* To characterize the capture process, the CO_2 removal efficiency and flux can be calculated using the equations below

$$\eta = \left(1 - \frac{C_{out}}{C_0}\right) \times 100\% \tag{7}$$

$$J_{CO_2} = \frac{273.15(C_0Q_0 - C_{out}Q_{out})}{22.4TS} \tag{8}$$

where η is the removal efficiency of CO_2, C_{out} is the outlet concentration of CO_2, C_0 denotes the inlet concentration of CO_2, J_{CO_2} is the CO_2 flux, Q_0 is the inlet volumetric flow rate, Q_{out} is the outlet volumetric flow rate, T is the operating temperature, and S is the membrane area, respectively. C_{out} is obtained by integrating the local concentration at the outlet of the shell side

$$C_{out} = \frac{\iint_{z=0} C(r)\, dA}{\iint_{z=0} dA} \tag{9}$$

The gas velocity is a key factor for CO_2 absorption using a HFMC. As illustrated in Figure 5, the effects of gas velocity on membrane performance are investigated. The removal efficiencies of CO_2 for five absorbents have a downward trend in Figure 5A. This is due to the reason that the residence time shortens with increasing gas velocity, which is unfavorable for the CO_2 capture process.[35] Additionally, the CO_2 removal efficiencies of H_2O and TEA are much lower than those of the other three solutions. Figure 5B illustrates that the flux of CO_2 increases with increasing gas velocity. This can be explained by the enhancement of the mass-transfer process in the HFMC. The mass-transfer resistance increases and the layer of the gas phase reduces with increasing the velocity of the gas mixture. In addition, it can be seen from Figure 5C that all of the five absorbents show similar behaviors in the purified CH_4 percentage. A lower gas velocity has a positive effect on the biogas purification. The CH_4 concentrations of PA and MEA reach 100% at the gas velocity of 0.19 m s^{-1}. Figure 5 also reveals that the simulation results are in good accordance with the available experimental data.

4.3.2. Effect of the Liquid Velocity. The effects of the liquid velocity on the membrane performance are illustrated in the velocity range of 0.046−0.08 m s^{-1} in Figure 6. With the increase in solvent velocity, the CO_2 removal process is enhanced. In this case, the CO_2 concentration gradient between the tube side and shell side increases with increasing liquid velocity. As plotted in Figure 6A, the separation efficiencies of H_2O and TEA have a slight change because of physical absorption and a low chemical reaction rate. On the other hand, a smaller liquid velocity reduces the liquid phase layer and the total resistance for mass transfer.[8] Therefore, the CO_2 flux increases for all absorbents with an increase of absorbent velocity. The reported phenomenon can be observed from Figure 6B. With respect to this figure, it can be concluded that a higher liquid velocity is good for CO_2 capture. For CO_2 flux, the comparison between modeling results and experimental data is also investigated using four chemical solutions as absorbents in Figure 6B.

4.3.3. Effect of the CO_2 Content. The changes of fermenting materials always cause the variation of the components of biogas in industrial applications. The effect of the CO_2 content from 30 to 50% on the HFMC performance in the presence of different aqueous solutions is shown in Figure 7. It is clearly seen that the removal efficiency of CO_2 decreases when the CO_2 content increases in Figure 7A. This is due to the fact that more unreacted CO_2 flows out of the module with a higher content of CO_2 in the gas mixture.[41] Moreover, PA solution shows better CO_2 capture

dx.doi.org/10.1021/ef501435q | Energy Fuels 2014, 28, 5745−5755

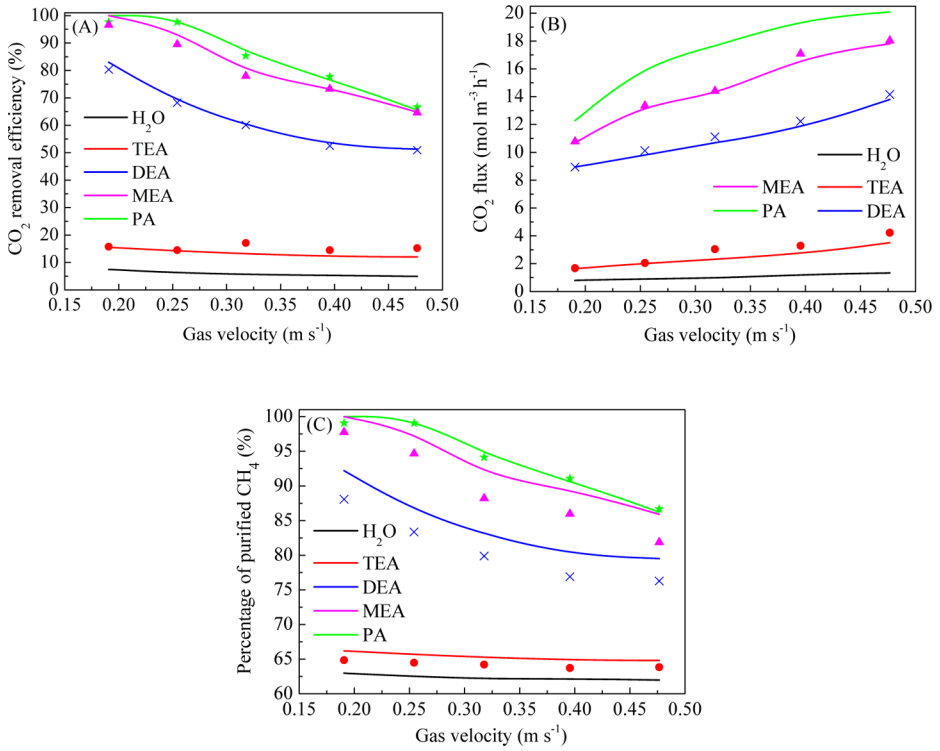

Figure 5. Effect of the gas velocity on the membrane performance (lines, simulation results, symbols, experimental data;[4] liquid concentration, 10 wt %; T, 303 K; and U_l, 0.06 m s^{-1}).

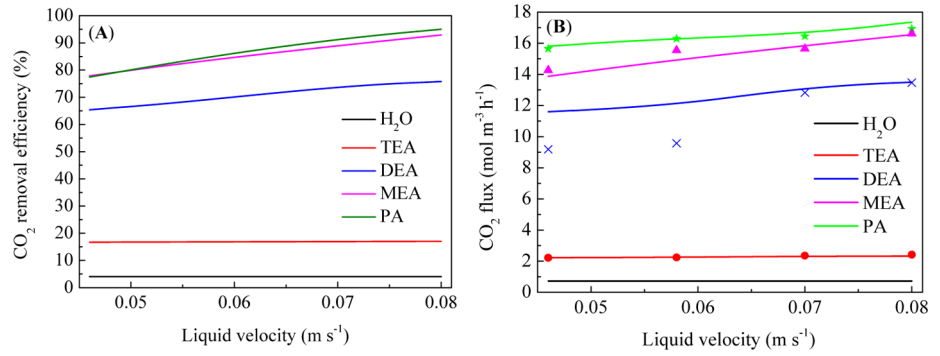

Figure 6. Effect of the liquid velocity on the membrane performance (lines, simulation results, symbols, experimental data;[4] liquid concentration, 20 wt %; T, 303 K; and U_g, 0.32 m s^{-1}).

efficiency within the scope of the CO_2 content. Even at a high CO_2 content of 50%, the corresponding CO_2 removal efficiency is 86.4%, which shows good membrane performance. In the meantime, it turns out that the CH_2 concentration declines, while the CO_2 content increases. As demonstrated in Figure 7B, the CO_2 flux grows up with the augment of the CO_2 concentration in the feed gas. This is due to the reason that a higher CO_2 concentration improves the driving force for the mass-transfer process of gas. As observed, there is a good agreement between the reported experimental data[4] and simulation results.

4.3.4. Effect of the Liquid Concentration. Figure 8 presents the influence of the solvent concentration (5, 10, 20, and 30 wt %) on the membrane performance. Chemical absorbents show better membrane performance, and the absorption performance of physical solution remains the same with the increase in the liquid concentration. As shown in panels A and C of Figure 8, both CO_2 absorption efficiency and CH_4 concentration after purification reach about 90% when using 30 wt % DEA, MEA, and PA solutions. Also, the CO_2 flux gradually increases with an increase of the liquid concentration because of a higher chemical reaction rate. The numerical observation is in perfect agreement with experimental data.[8,42] As observed, the change in the liquid concentration has a major positive effect on the biogas purification for solutions of MEA, MEA, and PA. For instance, when considering PA as the absorbent, the simulated percentage of CO_2 removal, CO_2 flux, and percentage of purified CH_4 increase from 61.6%, 11.58 mol m^{-3} h^{-1}, and 84.6% to 97.4%, 18.4 mol m^{-3} h^{-1}, and 99.0%, respectively.

4.4. Effect of the Membrane Structure. *4.4.1. Effect of the Fiber Diameter.* Figure 9 shows the effect of the fiber diameter on the contactor performance. As seen, bigger fibers provide better absorption performance. Under this condition, more solutions react with CO_2 in the tube side, which benefits the CO_2 capture.[43] As illustrated in Figure 9A, the CO_2 capture efficiencies of 240 μm fiber are about twice of those of 400 μm fiber. At the same time, the purified CH_4 concentration

dx.doi.org/10.1021/ef501435q | Energy Fuels 2014, 28, 5745−5755

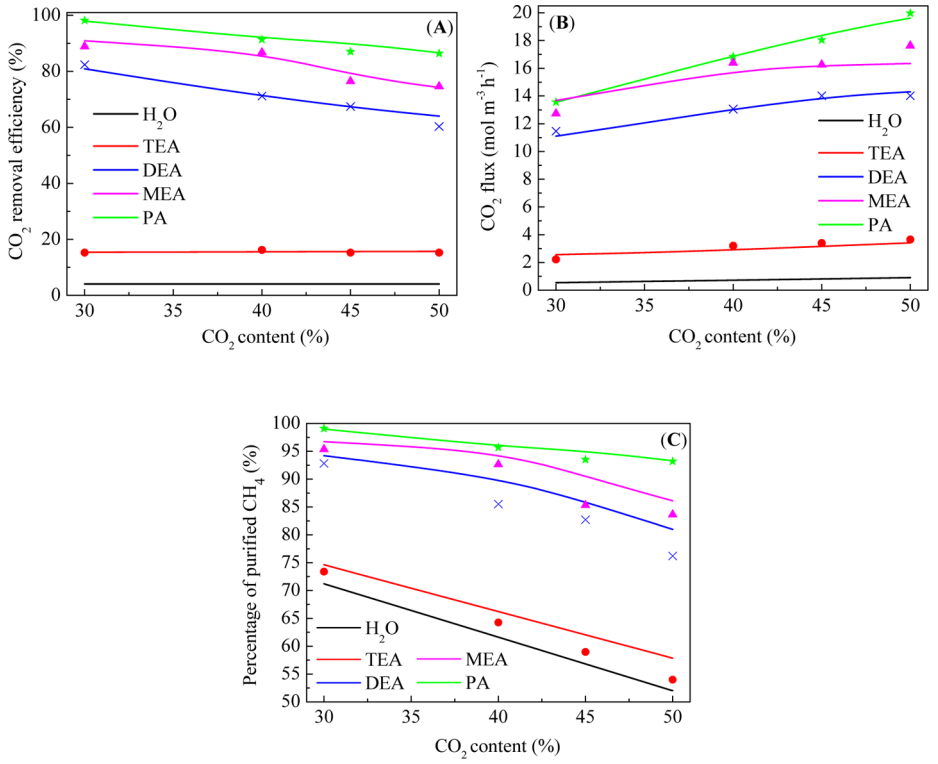

Figure 7. Effect of the CO_2 content on the membrane performance (lines, simulation results, symbols, experimental data;[4] liquid concentration, 20 wt %; T, 303 K; U_l, 0.06 m s^{-1}; and U_g, 0.32 m s^{-1}).

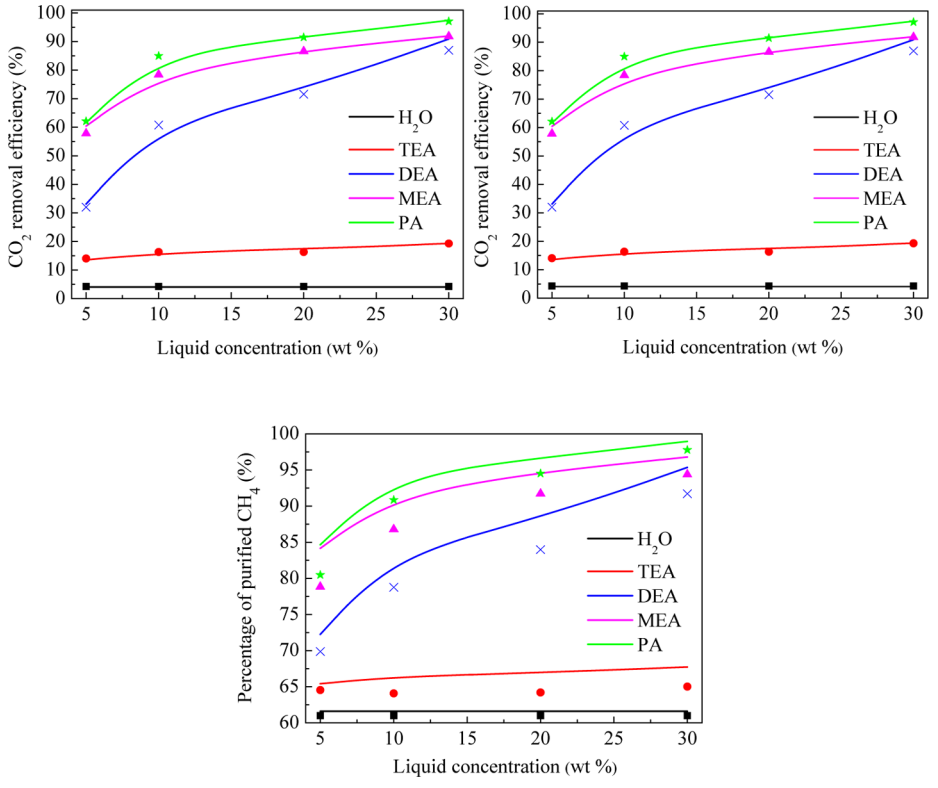

Figure 8. Effect of the liquid concentration on the membrane performance (lines, simulation results, symbols, experimental data;[4] T, 303 K; U_l, 0.06 m s^{-1}; and U_g, 0.32 m s^{-1}).

significantly increases with an increase in the diameter of the membrane fiber. On the other hand, the liquid velocity increases when a hollow fiber membrane with a smaller inner diameter is considered. As demonstrated in panels B and C of Figure 9, the CO_2 flux and CH_4 concentration after biogas upgrading also considerably increase.

dx.doi.org/10.1021/ef501435q | *Energy Fuels* 2014, 28, 5745−5755

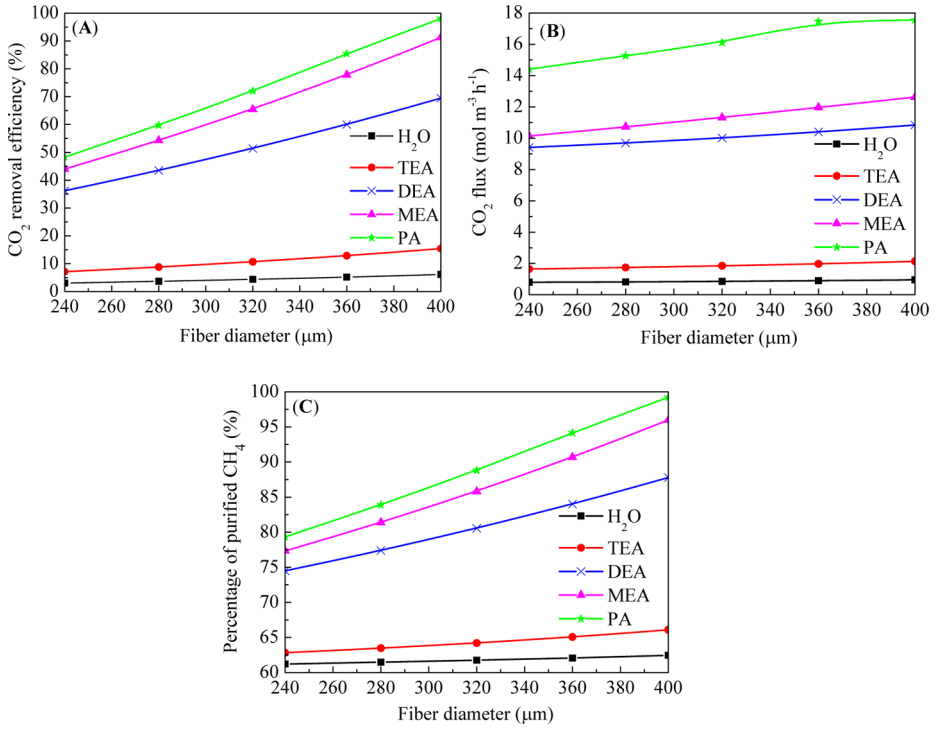

Figure 9. Effect of the fiber diameter on the membrane performance (liquid concentration, 10 wt %; T, 303 K; U_l, 0.06 m s^{-1}; and U_g, 0.32 m s^{-1}).

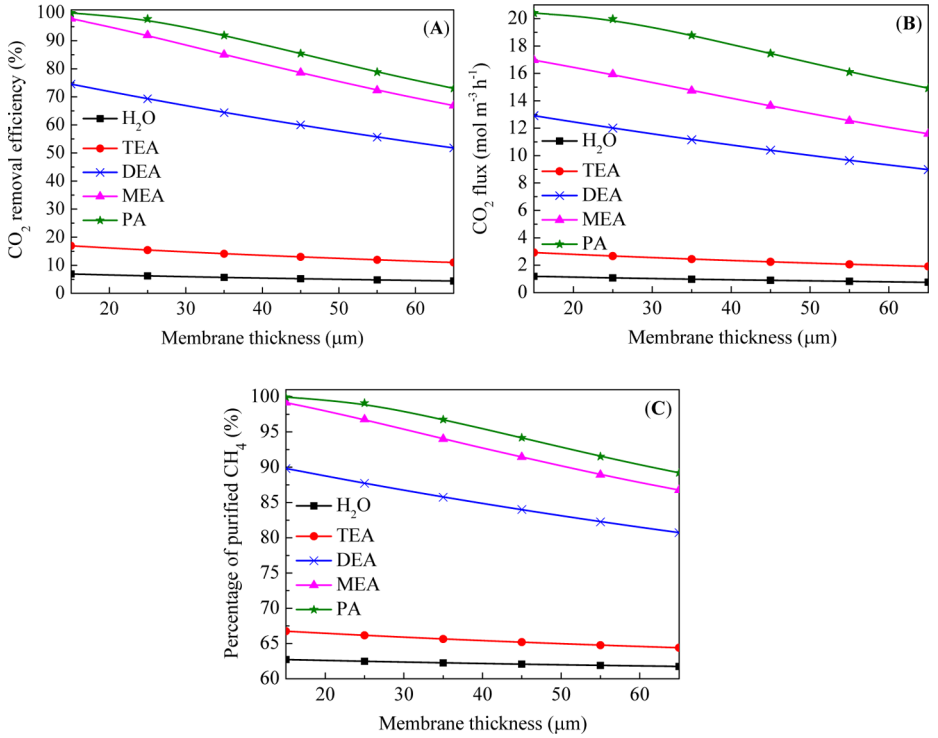

Figure 10. Effect of the membrane thickness on the membrane performance (liquid concentration, 10 wt %; T, 303 K; U_l, 0.06 m s^{-1}; and U_g, 0.32 m s^{-1}).

4.4.2. Effect of the Membrane Thickness. Figure 10 depicts the absorption performance of the membrane as a function of the membrane thickness. The thickness in the range from 15 to 65 μm is observed. Considering this figure, CO_2 removal efficiency and flux and CH_4 concentration at given conditions have a downward trend with increasing the thickness of the membrane. This is attributed to the increase of resistance along the pores with a thicker membrane.[43] With thinner thicknesses of membrane, the HFMC achieves a higher contactor performance. As observed in panels A and B of Figure 10, the percentages of captured CO_2 and purified CH_4 are higher than 97 and 99% using MEA and PA solutions in the hollow fiber module, respectively.

4.4.3. Effect of the Fiber Length. It is noted that the increase in the membrane module length enhances the biogas upgrading

dx.doi.org/10.1021/ef501435q | Energy Fuels 2014, 28, 5745−5755

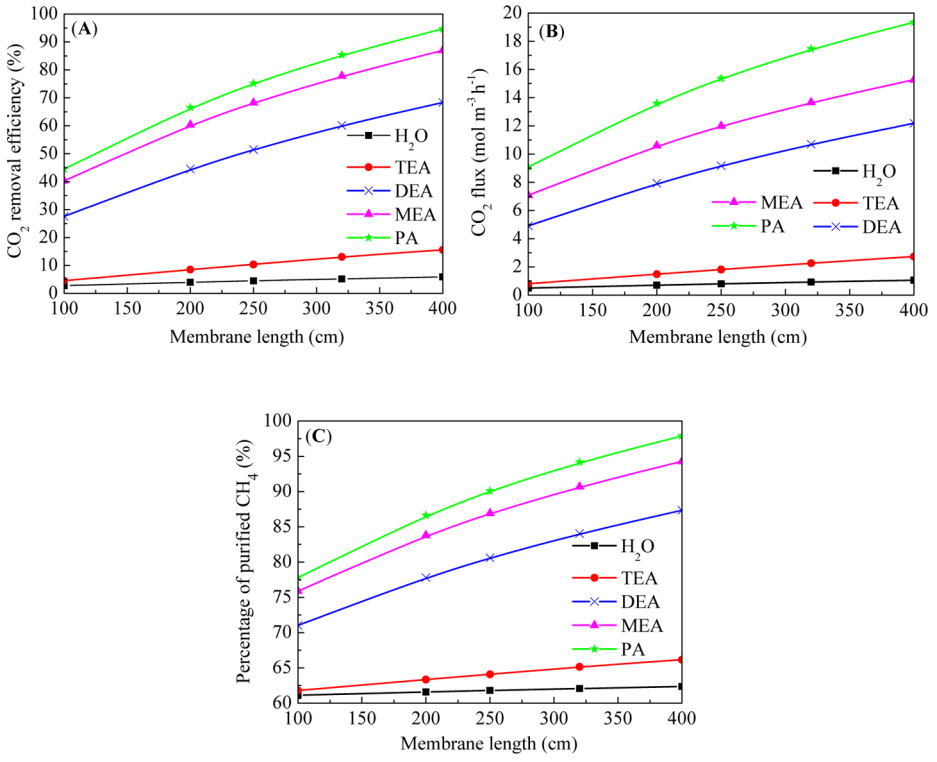

Figure 11. Effect of the fiber length on the membrane performance (liquid concentration, 10 wt %; T, 303 K; U_l, 0.06 m s^{-1}; and U_g, 0.32 m s^{-1}).

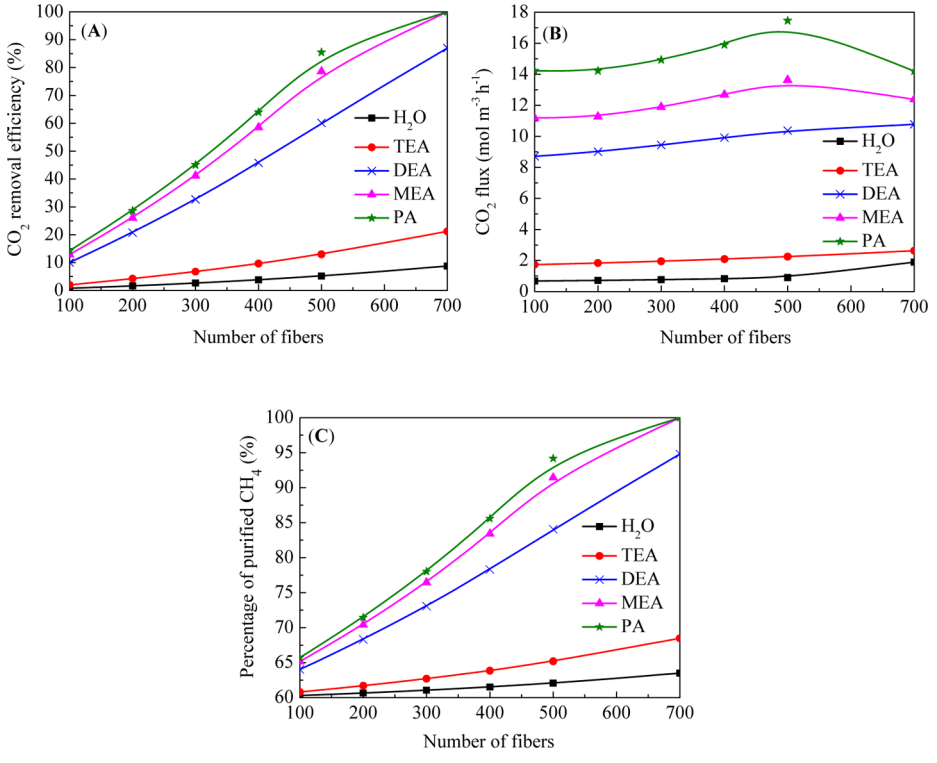

Figure 12. Effect of the number of fibers on the membrane performance (liquid concentration, 10 wt %; T, 303 K; U_l, 0.06 m s^{-1}; and U_g, 0.32 m s^{-1}).

process in Figure 11. The concentrations and velocities of gas and liquid are kept constant in this simulation. For a long fiber module, it offers more space for reaction between CO_2 and solution. The reacting time for gas and liquid is high enough, resulting in saturated aqueous solutions at the outlet of the contactor.[44] For example, when using PA solution as the absorbent, the CO_2 absorption efficiency and flux significantly increase by 50.2% and 10.3 mol m^{-3} h^{-1} with the increment of the hollow fiber module length in the range of 100−400 cm, respectively. In the meantime, the CH_4 content in the production of upgrading biogas also remarkably increases by 20.1%. Although increasing the module length improves the removal

dx.doi.org/10.1021/ef501435q | Energy Fuels 2014, 28, 5745−5755

performance, the costs on the fabrication of membrane contactors simultaneously increase. Thus, the absorption performance and economy should be taken into consideration in the design and selection of optimum module dimensions.

4.4.4. Effect of the Number of Fibers. Figure 12 reveals the effect of the number of fibers on the HFMC performance. As the number of fibers increases from 100 to 700, both the CO_2 removal efficiency and CH_4 concentration increase. Especially for these solvents that have a high reaction rate with CO_2, the two values increase roughly 90 and 35%, respectively. This is due to the fact that increasing the number of fibers results in a higher gas−liquid contact area and residence time inside the module. In addition, it is noted that the maximum of CO_2 flux coincides with the initial fiber dimensions of 500 fibers when using MEA and PA as absorbents. This can be explained by the simultaneous effect of the increased amount of absorbed CO_2 and the growth of the mass-transfer interface, which is illustrated by S in eq 8. Further, this phenomenon occurs also because the two solvents have a higher reaction rate with CO_2. However, the amount of fibers is limited and could be perfectly embedded in the module.

5. CONCLUSION

The aim of the present study was to study the potential interest of a membrane absorption process for CO_2 capture in biogas. A comprehensive 2D mass-transfer model was developed and solved considering non-wetted conditions for a countercurrent gas−liquid flow arrangement in the HFMC. Five kinds of absorbents (H_2O, TEA, DEA, MEA, and PA) were performed in the simulations. The established model showed excellent predictions, with experimental data reporting the influences of different gas and liquid parameters on the performance of the membrane contactor. Thus, the proposed model was capable of predicting the CO_2 absorption and CH_4 recovery processes in a hollow fiber membrane module. The key findings in this study are listed as follows: (1) The influences of gas and absorbent solution parameters on the membrane performance have been thoroughly investigated. One of the key results provided that increasing the gas velocity and CO_2 content decreased CO_2 removal efficiency and CH_4 recovery and increased CO_2 flux; in contrast, the increases in the absorbent velocity and concentration enhanced the membrane performance. (2) According to the results from the simulations, a smaller fiber inner diameter and membrane thickness and a longer module length were good for the biogas upgrading process. Particularly, it was found that the highest CO_2 flux coincided with the original fiber dimensions of 500 fibers when using MEA and PA as absorbents. This was due to the simultaneous effect of the increased amount of absorbed CO_2 and growth of the mass-transfer interface. (3) It was also indicated that PA provided better purification performance of the contactor than other absorbents. The order for CO_2 absorption efficiency and CH_4 recovery was PA > MEA > DEA > TEA > H_2O. Therefore, PA solution was proven as an advantageous aqueous solvent for capturing CO_2. (4) Among all of the factors of membrane properties, the fiber number, contactor length, and inner fiber diameter had a significant effect on the biogas upgrading process compared to the membrane thickness. This was due to the reason that the mass-transfer process of gas and absorbent dramatically enhanced. With regard to the parameters of the fluid, the liquid concentration and gas velocity were the major influences under these testing conditions. To obtain higher CH_4 production purity, the experiment should be operated at lower velocity of the gas phase and higher liquid concentration, which were beneficial to the absorption of CO_2.

AUTHOR INFORMATION

Corresponding Author

*Telephone: +862365103114. Fax: +862365111832. E-mail: yunfeiyan@cqu.edu.cn.

Author Contributions

†Yunfei Yan and Zhien Zhang contributed equally to this study and share first authorship.

Notes

The authors declare no competing financial interest.

ACKNOWLEDGMENTS

The authors gratefully acknowledge financial support from the Fundamental Research Funds for the Central Universities (CDJZR14145501), the National Natural Science Foundation of China (50906103), the Chongqing Science and Technology Talent Training Plan (cstc2013kjrc-qnrc90002), and the China National Tobacco Corporation Chongqing Branch (NY20130501010010).

NOMENCLATURE

C = concentration (mol m^{-3})
D = diffusion coefficient (m^2 s^{-1})
J = flux (mol m^{-2} h^{-1})
k = reaction rate constant (m^3 mol^{-1} s^{-1})
L = fiber length (cm)
n = number of fibers
Q = volumetric flow rate (m^3 s^{-1})
r = radial coordinate (μm)
R = gas constant (m^3 atm mol^{-1} K^{-1})
R_i = overall reaction rate of any species (mol m^{-3} s^{-1})
T = temperature (K)
U = velocity (m s^{-1})
$\bar{U}$ = average velocity (m s^{-1})

Greek Letters

ε = porosity
τ = tortuosity
θ = packing density
δ = membrane thickness (m)
η = CO_2 removal efficiency (%)

Subscripts

g = gas
l = liquid
mem = membrane
out = outlet

REFERENCES

(1) Makaruk, A.; Miltner, M.; Harasek, M. *Sep. Purif. Technol.* **2010**, *74*, 83−92.
(2) Rongwong, W.; Boributh, S.; Assabumrungrat, S.; Laosiripojana, N.; Jiraratananon, R. *J. Membr. Sci.* **2012**, *392*−*393*, 38−47.
(3) Yan, S. P.; Chen, J. A.; Ai, P.; Wang, Y. Y.; Zhang, Y. L. *Trans. Chin. Soc. Agric. Eng.* **2012**, *11*, 196−204.
(4) Zhang, Z. E.; Yan, Y. F.; Zhang, L.; Ju, S. X. *Global NEST J.* **2014**, *16*, 355−374.
(5) Wang, Z.; Fang, M.; Yu, H.; Ma, Q.; Luo, Z. *Energy Fuels* **2013**, *27*, 6887−6898.
(6) Masoumi, S.; Keshavarz, P.; Ayatollahi, S.; Mehdipour, M.; Rastgoo, Z. *Energy Fuels* **2013**, *27*, 5423−5432.
(7) Boributh, S.; Assabumrungrat, S.; Laosiripojana, N.; Jiraratananon, R. *J. Membr. Sci.* **2011**, *380*, 21−33.
(8) Zhang, Z. E.; Yan, Y. F.; Zhang, L.; Ju, S. X. *Int. J. Chem. Eng.* **2014**, *2014*, 1−7.

(9) Mehdipour, M.; Karami, M. R.; Keshavarz, P.; Ayatollahi, S. *Energy Fuels* **2013**, *27*, 2185−2193.
(10) Keshavarz, P.; Ayatollahi, S.; Fathikalajahi, J. *J. Membr. Sci.* **2008**, *325*, 98−108.
(11) Marzouk, S. A. M.; Al-Marzouqi, M. H.; El-Naas, M. H.; Abdullatif, N.; Ismail, Z. M. *J. Membr. Sci.* **2010**, *351*, 21−27.
(12) Marzouk, S. A. M.; Al-Marzouqi, M. H.; Abdullatif, N.; Ismail, Z. M. *J. Membr. Sci.* **2010**, *360*, 436−441.
(13) Porcheron, F.; Drozdz, S. *Chem. Eng. Sci.* **2009**, *64*, 265−275.
(14) Rangwala, H. A. *J. Membr. Sci.* **1996**, *112*, 229−240.
(15) Lin, S. H.; Chiang, P. C.; Hsieh, C. F.; Li, M. H.; Tung, K. L. *J. Chin. Inst. Chem. Eng.* **2008**, *39*, 13−21.
(16) Muñoz, D. M.; Portugal, A. F.; Lozano, A. E.; de la Campa, J. G.; de Abajo, J. *Energy Environ. Sci.* **2009**, *2*, 883.
(17) Kumar, P. S.; Hogendoorn, J. A.; Feron, P. H. M.; Versteeg, G. F. *Chem. Eng. Sci.* **2002**, *57*, 1639−1651.
(18) van Holst, J.; Kersten, S. R. A.; Hogendoorn, K. J. A. *J. Chem. Eng. Data* **2008**, *53*, 1286−1291.
(19) Keshavarz, P.; Fathikalajahi, J.; Ayatollahi, S. *J. Hazard. Mater.* **2008**, *152*, 1237−1247.
(20) Shirazian, S.; Pishnamazi, M.; Rezakazemi, M.; Nouri, A.; Jafari, M.; Noroozi, S.; Marjani, A. *Chem. Eng. Technol.* **2012**, *35*, 1077−1084.
(21) Al-Marzouqi, M. H.; El-Naas, M. H.; Marzouk, S. A. M.; Al-Zarooni, M. A.; Abdullatif, N.; Faiz, R. *Sep. Purif. Technol.* **2008**, *59*, 286−293.
(22) Al-Marzouqi, M.; El-Naas, M.; Marzouk, S.; Abdullatif, N. *Sep. Purif. Technol.* **2008**, *62*, 499−506.
(23) Jung, H. J.; Han, S. H.; Lee, Y. M.; Yeo, Y. K. *Korean J. Chem. Eng.* **2011**, *28*, 1497−1504.
(24) Versteeg, G. F.; van Dijck, L. A. J.; van Swaaij, W. P. M. *Chem. Eng. Commun.* **1996**, *144*, 113−158.
(25) Happel, J. *AIChE J.* **1959**, *5*, 174−177.
(26) Hua, C. G.; Kang, G. D.; Jia, J. X.; Li, M.; Cao, Y. M.; Yuan, Q. *Chem. J. Chin. Univ.* **2013**, *34*, 906−912.
(27) Faiz, R.; El-Naas, M. H.; Al-Marzouqi, M. *Chem. Eng. J.* **2011**, *168*, 593−603.
(28) Shirazian, S.; Ashrafizadeh, S. N. *Sep. Sci. Technol.* **2010**, *45*, 515−524.
(29) Versteeg, G. F.; van Swaaij, W. P. M. *J. Chem. Eng. Data* **1988**, *33*, 29−34.
(30) Constantinou, A.; Barrass, S.; Gavriilidis, A. *Ind. Eng. Chem. Res.* **2014**, *53*, 9236−9242.
(31) Barth, D.; Tondre, C.; Delpuech, J. J. *Int. J. Chem. Kinet.* **1986**, *18*, 445−457.
(32) Cheng, M. D.; Caparanga, A. R.; Soriano, A. N.; Li, M. H. *J. Chem. Thermodyn.* **2010**, *42*, 342−347.
(33) Hikita, H.; Asai, S.; Ishikawa, H.; Honda, M. *Chem. Eng. J.* **1977**, *13*, 7−12.
(34) Park, S. W.; Choi, B. S.; Lee, J. W. *Korean J. Chem. Eng.* **2006**, *23*, 138−143.
(35) Shirazian, S.; Ashrafizadeh, S. N. *Sep. Sci. Technol.* **2010**, *45*, 515−524.
(36) Bosch, H.; Versteeg, G. F.; van Swaaij, W. P. M. *Chem. Eng. Sci.* **1990**, *45*, 1167−1173.
(37) van Holst, J.; Kersten, S. R. A.; Hogendoorn, K. J. A. *J. Chem. Eng. Data* **2008**, *53*, 1286−1291.
(38) Shen, S.; Feng, X.; Zhao, R.; Ghosh, U. K.; Chen, A. *Chem. Eng. J.* **2013**, *222*, 478−487.
(39) Perrin, D. *Dissociation Constants of Organic Acids and Bases*; Butterworths: London, U.K., 1965.
(40) Paul, S.; Thomsen, K. *Int. J. Greenhouse Gas Control* **2012**, *8*, 169−179.
(41) Boributh, S.; Assabumrungrat, S.; Laosiripojana, N.; Jiraratananon, R. *J. Membr. Sci.* **2011**, *372*, 75−86.
(42) Zhu, D.; Fang, M.; Lv, Z.; Wang, Z.; Luo, Z. *Energy Fuels* **2012**, *26*, 147−153.
(43) Zhang, Z. E.; Yan, Y. F.; Zhang, L.; Ju, S. X. *J. Nat. Gas Sci. Eng.* **2014**, *19*, 311−316.
(44) Boucif, N.; Favre, E.; Roizard, D. *Chem. Eng. Sci.* **2008**, *63*, 5375−5385.